Forecasting different types of avalanches based on snow depth and snowfall/snowmelt conditions on the southeastern Tibetan Plateau

Xiaoqian Fu[1,2], Jiansheng Hao[1,2,*], Peng Cui[1,2], Yan Wang[1,2], Guoqing Chen[1,2]

[1]Key Laboratory of Mountain Hazards and Engineering Resilience, Institute of Geographic Sciences and Natural Resources Research, Chinese Academy of Sciences, Beijing 100101, China;
[2]College of Resources and Environment, University of Chinese Academy of Sciences, Beijing 101408, China;

Correspondence to: Jiansheng Hao (haojs@igsnrr.ac.cn)

Abstract. Reliable avalanche forecasting is essential for protecting mountain communities and transportation corridors, but estimating avalanche occurrence from monitored meteorological and snowpack conditions remains difficult. Operational assessments often rely primarily on meteorological thresholds, although avalanche responses depend on both type-specific triggering processes and snowpack conditions. Using meteorological, pre-event snow depth, and avalanche observations collected during the 2024 and 2025 snow seasons, we analysed 37 recorded avalanche events, together with corresponding non-avalanche periods. Separate logistic-regression models were developed for dry- and wet-snow avalanches using the intensity and duration of the preceding snowfall or snowmelt process and pre-event snow depth. Their performance was compared with otherwise identical models excluding snow depth. Under leave-one-out cross-validation, including pre-event snow depth increased the area under the receiver operating characteristic curve from 0.72 to 0.83 for dry-snow avalanches and from 0.85 to 0.94 for wet-snow avalanches. For wet-snow avalanches, the true-positive rate increased from 0.79 to 0.92, while the false-positive rate decreased from 0.21 to 0.13. These results indicate that pre-event snow depth provides additional discriminatory information beyond meteorological forcing alone, particularly for wet-snow avalanches, and supports the development of locally adapted avalanche assessment methods.

1 Introduction

Climate warming is altering snowfall regimes, snowmelt timing, and rain–snow transitions in mountain regions, thereby reshaping the environmental conditions associated with cryospheric hazards (Li et al., 2024). In high mountains, snow avalanches are among the most consequential gravity-driven natural hazards. Owing to their sudden release, rapid movement, and potentially long runout distances, avalanches pose persistent threats to mountain communities, transportation corridors, and critical infrastructure (Acharya et al., 2023). At the same time, the expansion of hydropower facilities and high-elevation transportation networks is increasing the exposure of people and infrastructure to avalanche hazards. This growing interaction between avalanche occurrence and socioeconomic exposure highlights the need for reliable monitoring and forecasting systems in mountain regions.

Avalanche forecasting requires a quantitative characterization of how meteorological forcing interacts with the snowpack to influence the probability of avalanche release. However, the dominant triggering processes and failure mechanisms vary among avalanche types. Dry-snow avalanches, which predominantly occur under sub-freezing conditions, are often associated with rapid new-snow accumulation and the resulting increase in load on the pre-event snowpack (McClung, 2009; Schweizer et al., 2003b). For dry-snow slab avalanches, this additional loading can promote failure in a weak layer and subsequent crack propagation through the snowpack, eventually resulting in slab release. Consequently, cumulative new snow and snowfall intensity are commonly used as key indicators in the assessment and forecasting of dry-snow avalanche hazard (Wei et al., 2025). Empirical studies in the Swiss Alps have reported a substantial increase in avalanche probability when 1–3 d cumulative new-snow amounts reach approximately 30–50 cm (Schweizer et al., 2003a). Beyond fixed empirical thresholds, recent studies have increasingly evaluated the balance between meteorological loading and snowpack stability to improve probabilistic predictions of natural dry-snow avalanche activity (Mayer et al., 2023).

In contrast, wet-snow avalanches typically occur during periods of sustained warming, rain-on-snow events, or active snowmelt. As air temperature rises and liquid water enters the snowpack, water infiltration alters grain-scale bonding, enhances snow deformation, and may lead to water accumulation along stratigraphic interfaces. Together, these processes reduce snowpack strength and promote wet-snow instability and avalanche release (Hendrick et al., 2023; Mayer et al., 2024). Consequently, air-temperature evolution, surface energy input, and liquid-water availability are commonly used as predictors of wet-snow avalanche activity (Bellaire et al., 2017). A two-decade observational record from the Dischma Valley, Switzerland, showed that natural wet-snow avalanche activity was frequently preceded by 3–5 consecutive days with mean daily air temperatures above 0 °C (Baggi and Schweizer, 2009). From an energy-balance perspective, observations in the Davos region indicated that a cumulative positive net energy input of approximately 1.2 MJ m^{-2} over 3 d was associated with periods of widespread wet-snow avalanche activity (Mitterer and Schweizer, 2013). Furthermore, analyses of long-term observational records in North America showed that, during sustained spring warming, liquid-water percolation and its accumulation above persistent weak layers may contribute to the release of large wet-snow avalanches (Marienthal et al., 2015). Nevertheless, although these meteorological indicators capture important aspects of wet-snow avalanche formation, their predictive performance may vary substantially among locations and snowpack conditions, resulting in false alarms and missed events when fixed thresholds are applied (Morin et al., 2020).

This limitation arises because avalanche release depends not only on meteorological forcing but also on snowpack conditions, which vary substantially across space and time (Schweizer et al., 2003a, 2008). Consequently, similar snowfall or melt forcing can produce contrasting stability responses under different snowpack conditions. Fixed meteorological thresholds may therefore fail to capture this state dependence, resulting in false alarms or missed events. The importance of snowpack information for avalanche forecasting has long been recognised (LaChapelle, 1980), including in earlier forecasting models (Schweizer and Föhn, 1996). More recent studies have shown that combining meteorological observations with snowpack process simulations can improve avalanche prediction relative to meteorology-only approaches (Pérez-Guillén et al., 2022). These findings highlight the value of incorporating indicators of the snowpack condition into avalanche forecasting models.

Focusing on an avalanche-prone high mountain valley in the southeastern Tibetan Plateau, this study compiles an event database using a dedicated in situ monitoring network that integrates meteorological, snow depth, and avalanche observations. Pre-event snow depth is defined as the snow depth at the onset of the preceding snowfall or snowmelt process. Separate logistic regression models are developed for dry- and wet-snow avalanches to quantify the relationships between forcing intensity, forcing duration, pre-event snow depth, and avalanche occurrence. These models are compared with meteorology-only baselines to assess whether the inclusion of pre-event snow depth improves event discrimination and reduces false-alarm rates. By incorporating observed pre-event snow depth into type-specific logistic regression models, this study provides an interpretable quantitative basis for regional avalanche monitoring and forecasting.

2. Study area and data

2.1 Study area

Galongla Valley is located on the southeastern margin of the Tibetan Plateau, China, within the lower Yarlung Zangbo River basin (Fig. 1a). The region lies along a major monsoonal moisture-transport pathway, through which moisture from the Bay of Bengal is transported northward via the Yarlung Zangbo Grand Canyon, contributing substantially to precipitation along the canyon corridor (Yuan et al., 2023). Elevation within the study area ranges from 2723 to 5699 m. The terrain is steep and deeply dissected, with a mean slope angle of approximately 34° and maximum values exceeding 70°. Numerous confined gullies connect high-elevation snow accumulation areas with the valley floor and adjacent transportation corridors, providing favourable topographic conditions for avalanche release and channelised downslope movement. The main snow season generally extends from late December to June, and the local snow regime exhibits pronounced characteristics of a maritime snow climate (Wen et al., 2024). Frequent snowfall, episodic warming, and recurrent melt–freeze conditions produce substantial temporal changes in snowpack properties, creating favourable conditions for both snowfall-induced dry-snow avalanches and snowmelt-induced wet-snow avalanches. Galongla Valley was therefore selected as a representative site for integrated observations of meteorological, snowpack, and avalanche activity. Field investigations identified 23 avalanche paths, 12 of which directly threaten local transportation routes (Fig. 1b). To systematically monitor avalanche activity and its environmental controls, an integrated network of ten monitoring stations was deployed near the release zones of the avalanche paths posing the greatest threat to infrastructure (Fig. 1b, 1c).

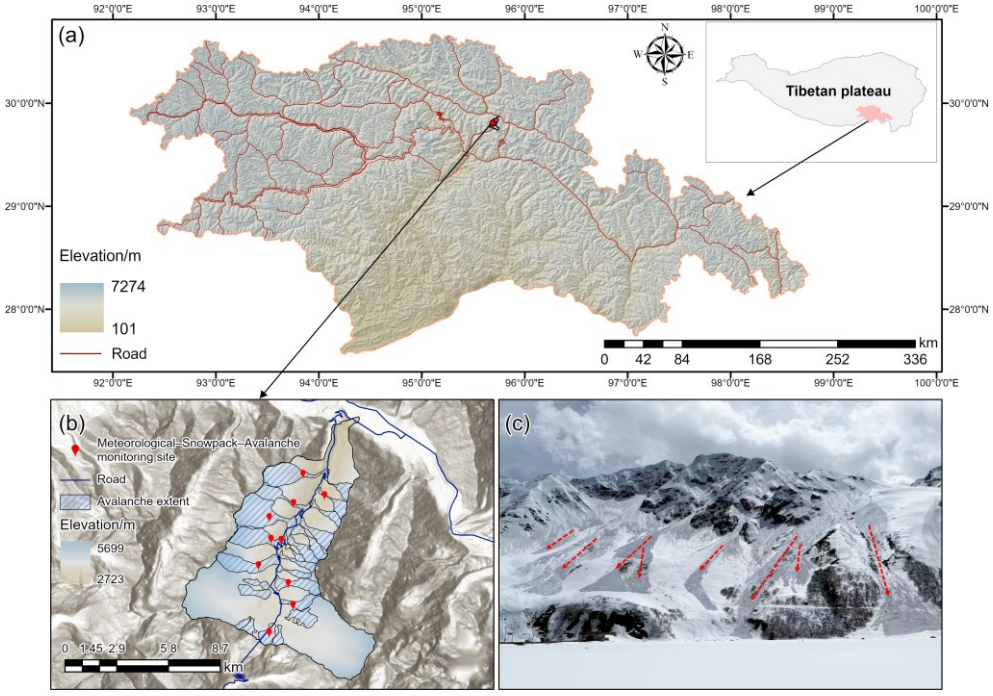


Figure 1. Overview of the study area and monitoring network. (a) Regional topography of the southeastern Tibetan Plateau, China, showing the location of the Galongla Valley. (b) Distribution of monitoring stations and mapped avalanche extents within the Galongla Valley. (c) Field photograph of Galongla Mountain showing avalanche paths.

2.2 Data

The meteorological and snowpack data used in this study were obtained from an integrated meteorological–snowpack–avalanche monitoring network that has been operating in the Galongla Valley since 2023 (Fig. 2a). The stations are strategically located near the potential release zones of major avalanche-prone slopes at elevations of 3600–3700 m, enabling the effective capture of key meteorological forcing and snowpack evolution processes within avalanche release areas. Each station consists of an automatic weather station, a weighing precipitation gauge, a snow stake, and a thermal infrared camera (Fig. 2b), with meteorological and snow-depth variables recorded at a temporal resolution of 1 min. The predictor variables were calculated from hourly records derived from these observations. During the snow season, avalanche events affecting transportation corridors and adjacent slopes are documented in real time using integrated video surveillance systems, allowing for the systematic collection of essential event information, including occurrence time and avalanche type.

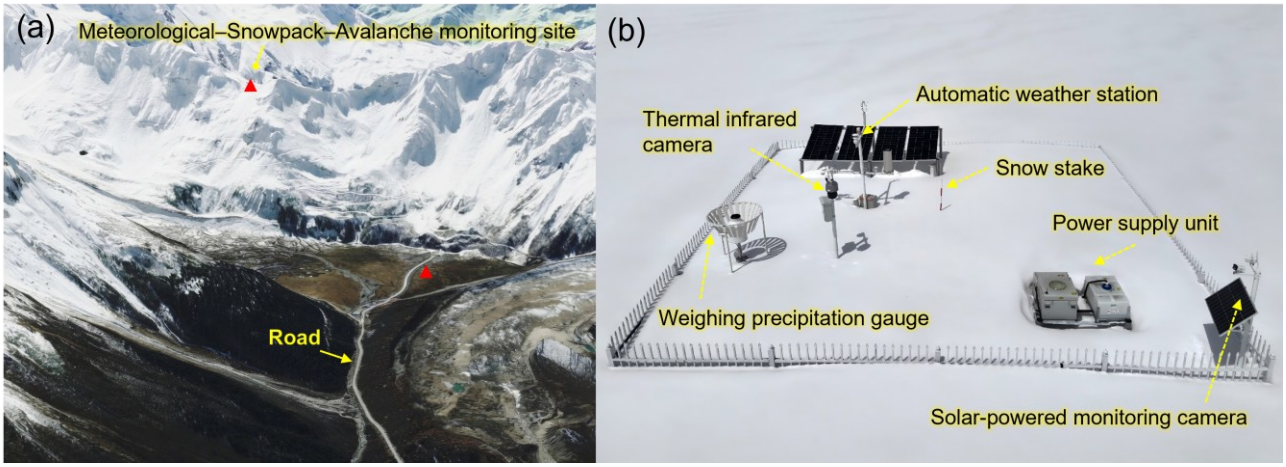


Figure 2. Integrated meteorological–snowpack–avalanche monitoring system in Galongla Valley. (a) Locations of representative monitoring stations; (b) Field configuration of the monitoring network.

2.3 Predictor variables

Dry-snow avalanches predominantly occur under subfreezing conditions, typically following intense snowfall during sustained cold periods. The primary triggering mechanism is rapid mechanical loading caused by the accumulation of new snow. Under these conditions, snow grains are generally dry and unconsolidated, with weak intergranular bonding. Upon release, dry-snow avalanches can reach velocities of several tens of metres per second and propagate as powder-snow clouds or highly fragmented dense flows along steep avalanche paths (Fig. 3a), before depositing in runout zones where they may block transportation corridors (Fig. 3b). Consequently, snowfall is recognised as the principal driver of dry-snow avalanche initiation. To quantitatively characterise this dynamic loading process, we define a snowfall event as a continuous period with measurable snowfall and a concurrent increase in snow depth. For avalanche samples, the triggering process was defined as the last snowfall event preceding the recorded avalanche occurrence time (t_{event}), and any ongoing snowfall event was cut off at t_{event}. Using hourly records, snowfall duration (SFD) was calculated as the duration of this event segment, and snowfall intensity (SFI) as the corresponding cumulative snowfall divided by SFD, representing the mean rate of snow loading. In parallel, the snow depth recorded at the onset of the event was defined as pre-event snow depth (SD).

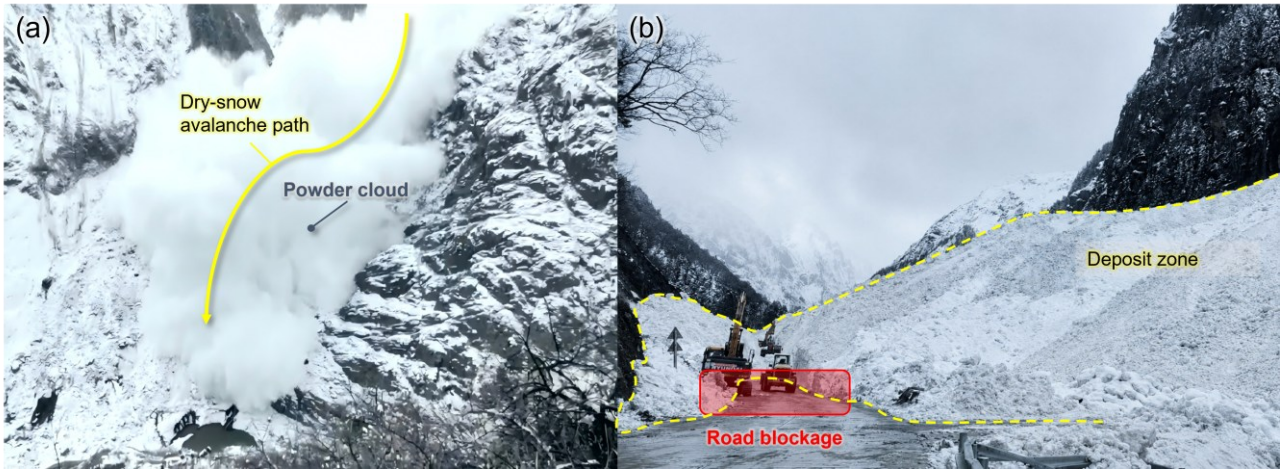


Figure 3. Typical movement and deposits of dry-snow avalanches. (a) Dry-snow avalanche path with a powder cloud; (b) Avalanche deposit causing road blockage.

Wet-snow avalanches predominantly occur during warming periods or rain-on-snow conditions, and are primarily triggered by rapid air-temperature increases or liquid-water input. The percolation of meltwater promotes snowpack structural weakening and reduces shear strength, thereby increasing the susceptibility of the slab to overall instability. Although wet-snow avalanches generally propagate at lower velocities than dry-snow avalanches, they often involve substantial mass and can exert persistent and destructive impact pressures. These events typically develop as dense, water-rich flows with a high capacity to entrain debris and ice fragments as they move downslope along confined avalanche paths (Fig. 4a). Owing to their high bulk density and large mass, wet-snow avalanches commonly form compact depositional masses in runout zones, which can severely obstruct roads and transportation corridors (Fig. 4b). Consequently, snowmelt is identified as a key driver of wet-snow avalanche initiation. In this study, we define a snowmelt event as a distinct period during which air temperature exceeds 0 °C and snow depth continuously decreases. For avalanche samples, the triggering process was defined as the last snowmelt event preceding t_{event}, and any ongoing snowmelt event was cut off at the avalanche occurrence time. Snowmelt duration (SMD) was calculated from hourly records as the duration of this event segment, whereas snowmelt intensity (SMI) was calculated as the corresponding cumulative snow-depth loss divided by SMD. Similarly, the snow depth recorded at the onset of the event was defined as pre-event snow depth (SD).

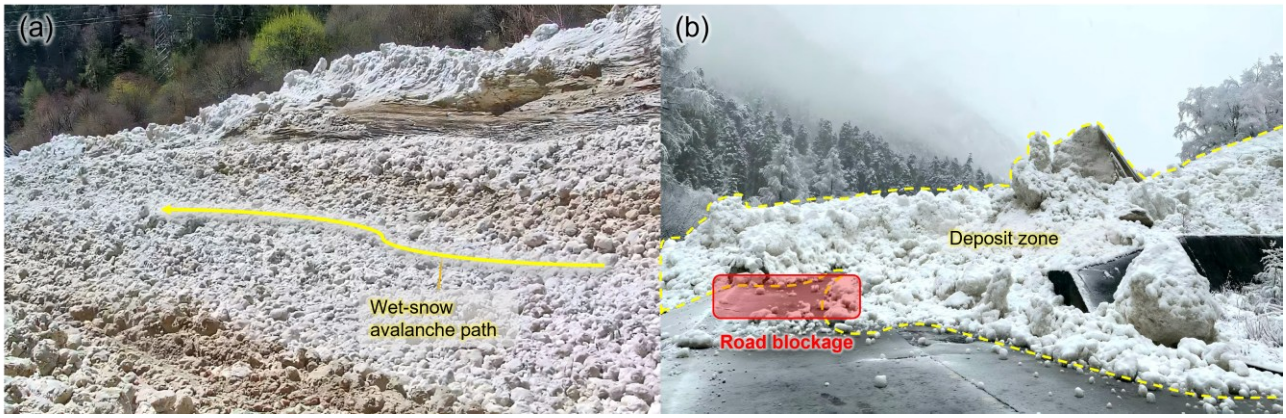


Figure 4. Typical movement and deposits of wet-snow avalanches. (a) Wet-snow avalanche path; (b) Avalanche deposit causing road blockage.

2.4 Construction of positive and negative samples

For each recorded dry- or wet-snow avalanche, candidate snowfall or snowmelt-related process blocks were identified within a 3-d retrospective window at the monitoring station geographically closest to the avalanche location using the same process-identification criteria described above. The most recent qualifying process block preceding the recorded avalanche time was treated as the positive sample, with all variables calculated only up to the avalanche occurrence time. Earlier process blocks within the same retrospective window were considered candidate negative samples. Candidate negative sample intervals were limited to a maximum duration of 6 h, even when the underlying processes lasted longer. Intervals overlapping the 12 h immediately preceding the start of the positive block were excluded, and eligible intervals closer to the positive block were prioritised. Candidate blocks overlapping any known avalanche occurrence at the same station and of the same avalanche type were also removed using the full avalanche-time inventory. Eligible negative samples were retained to achieve an overall positive-to-negative sample ratio of 1:3 for each avalanche type. Each candidate process block contributed at most one retained sample, although multiple blocks could originate from the same broader snowfall or snowmelt episode. The predictor variables for positive and negative samples were calculated over their respective retained intervals using identical definitions to ensure direct comparability. After screening, the dry-snow dataset comprised 13 positive and 39 negative samples, and the wet-snow dataset comprised 24 positive and 72 negative samples. Each retained process block was treated as one classification unit. An example of the sample-construction procedure is shown in Fig. 5.

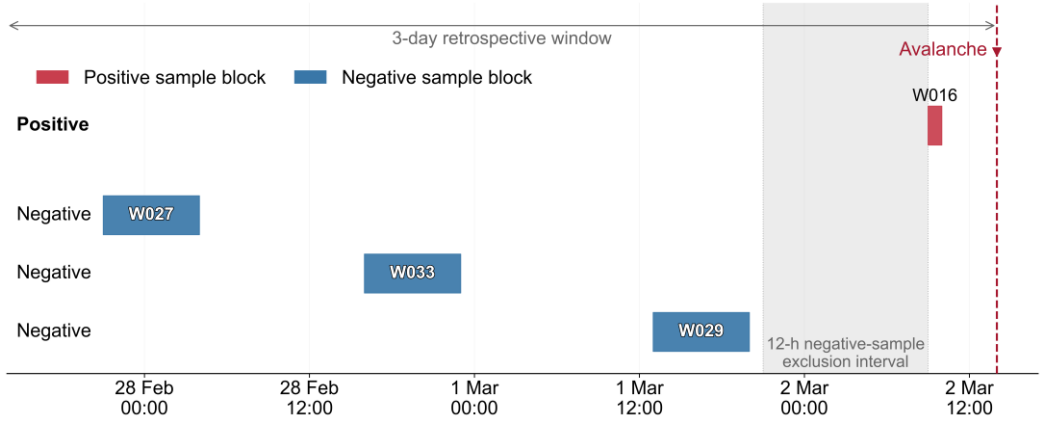


Figure 5. Example of the temporal construction of positive and negative samples using an observed wet-snow avalanche case. The red and blue blocks indicate the positive and retained negative samples, respectively. The grey shading represents the 12 h exclusion interval preceding the start of the positive block, and the red dashed line marks the recorded avalanche time.

2.5 Statistical modelling and performance evaluation

Within a statistical modelling framework, this study employs logistic regression (LR), which has previously been applied to avalanche forecasting (Gauthier et al., 2017), to develop an avalanche forecasting model that combines snowfall- or snowmelt-process variables with pre-event snow depth, hereafter referred to as the Snowpack–Meteorology Logistic Model (SMLM). For each avalanche type, the SMLM uses three predictor variables: forcing intensity, forcing duration, and pre-event snow depth, with avalanche occurrence or non-occurrence treated as the binary response variable (Fu et al., 2026). To reduce the influence of differences in physical magnitude and skewed variable distributions on parameter estimation, all input variables are subjected to a uniform logarithmic transformation before model fitting. The transformation is expressed as follows:

$$x_i' = \ln(1 + x_i)\,, \tag{1}$$

where x_i denotes the original input variable and x_i' denotes the transformed model input. In the space of log-transformed variables, the LR model is expressed as:

$$P(Y = 1 \mid x) = \frac{1}{1+\exp\left[-\left(b+\sum_{i=1}^{k} w_i x_i'\right)\right]}, \tag{2}$$

where $P(Y = 1 \mid x)$ represents the model-derived avalanche classification score for a sampled process block, w_i is the regression coefficient for the *i-th* input variable, b is the intercept term, and k is the number of input variables. Model parameters are estimated using maximum likelihood estimation.

To ensure the robustness and reliability of the parameter estimates, multicollinearity among the predictors was assessed using the variance inflation factor (VIF). All VIF values were below the threshold of 3, indicating no substantial multicollinearity among the predictors (Zuur et al., 2010). In addition, to quantify uncertainty in the model parameters, a non-parametric bootstrap procedure was applied. Specifically, 1000 bootstrap resamples were generated with replacement, and the regression coefficients were repeatedly estimated to derive their corresponding 95% confidence intervals (CIs). A predictor was

considered statistically significant at the 95% confidence level when its bootstrap-derived confidence interval did not include zero (Efron and Tibshirani, 1986).

The discriminative performance of the model was evaluated using leave-one-out cross-validation (LOOCV). In the LOOCV framework, one observation is withheld as the test sample in each iteration, whereas the remaining observations are used for model training. This procedure is repeated until out-of-fold classification scores and their corresponding ground-truth labels are obtained for all observations (Hastie et al., 2009). Based on these predictions, we constructed a receiver operating characteristic (ROC) curve and calculated the area under the ROC curve (AUC) to quantify the overall discriminative ability of the model. The optimal classification threshold was determined by maximising the Youden Index ($J = TPR - FPR$), where TPR and FPR denote the true positive rate and false positive rate (Youden, 1950). The classification scores were then converted into binary classifications using this optimal threshold, and a confusion matrix was constructed (Table 1). Based on this matrix, a comprehensive set of performance metrics was calculated to evaluate classification performance, including TPR, FPR, true negative rate (TNR), false negative rate (FNR), precision, the true skill statistic (TSS), and F1-score (Fawcett, 2006). The mathematical formulations for these metrics are detailed in Eqs. (3) – (9).

Table 1. Contingency matrix

	Observed	
Predicted	Yes	No
Yes	TP	FP
No	FN	TN

$$\mathrm{TPR} = \frac{\mathrm{TP}}{\mathrm{TP+FN}}, \tag{3}$$

$$\mathrm{FPR} = \frac{\mathrm{FP}}{\mathrm{FP+TN}}, \tag{4}$$

$$\mathrm{TNR} = \frac{\mathrm{TN}}{\mathrm{TN+FP}}, \tag{5}$$

$$\mathrm{FNR} = \frac{\mathrm{FN}}{\mathrm{TP+FN}}, \tag{6}$$

$$\mathrm{Precision} = \frac{\mathrm{TP}}{\mathrm{TP+FP}}, \tag{7}$$

$$\mathrm{TSS} = \mathrm{TPR} + \mathrm{TNR} - 1, \tag{8}$$

$$\mathrm{F1} = \frac{2\mathrm{TP}}{2\mathrm{TP+FP+FN}}, \tag{9}$$

To evaluate the contribution of pre-event snow depth to model discrimination, we constructed a baseline model driven exclusively by meteorological variables, hereafter referred to as the Meteorology-Only Logistic Model (MOLM). To ensure rigorous comparability, the integrated and baseline models were implemented using consistent definitions, model-construction procedures, and validation strategies. Specifically, the MOLM included the snowfall- or snowmelt-process predictors: SFI and SFD for dry-snow avalanches and SMI and SMD for wet-snow avalanches. The SMLM additionally included pre-event snow depth. To quantify uncertainty in model performance, 1000 paired bootstrap resamples of the LOOCV out-of-fold prediction

records were used to calculate percentile 95% confidence intervals for AUC, TPR, FPR, and TSS, as well as for the differences in AUC and TSS between the SMLM and MOLM.

3. Results

3.1 Avalanche activity characteristics

Based on monitoring data from two consecutive snow seasons (1 January–15 May in 2024 and 2025), we analysed mean snow depth and air temperature averaged across all monitoring stations in Galongla Valley (Fig. 6). During the 2024 snow season, the mean snow depth and mean air temperature were 0.17 m and -0.27 °C, respectively. In 2025, the corresponding values were 0.24 m and 1.16 °C. Overall, the main period of snow accumulation extended from January to March, with snow depth reaching seasonally high levels between late January and March. Thereafter, rising air temperatures were accompanied by rapid snow depletion, and the seasonal snow cover largely disappeared between April and May.

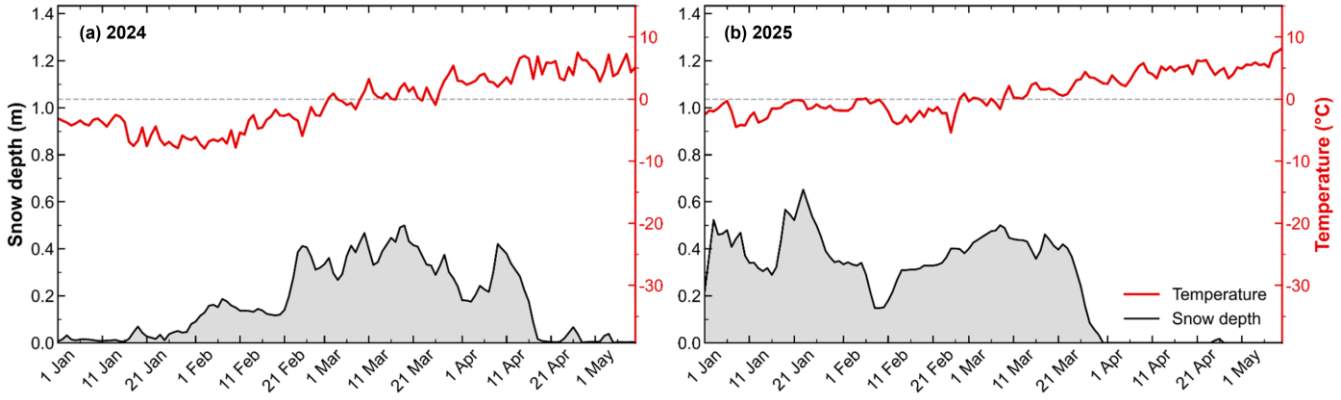


Figure 6. Time series of daily air temperature and snow depth in the Galongla Valley during the 2024 and 2025 snow seasons. The red lines represent air temperature (°C), and the grey shaded areas indicate snow depth (m).

Consistent with the observed snowpack evolution, avalanche activity showed a concentrated seasonal distribution. During the 2024 and 2025 snow seasons, the monitoring network documented 37 avalanche events in total. Overall, avalanche activity was concentrated from late February to mid-April, peaked during the first half of March, declined during the second half of March, and was not recorded after mid-April (Fig. 7). The two avalanche types differed primarily in the duration of their seasonal occurrence. Dry-snow avalanches (n = 13) occurred from late February to the end of March, with the highest frequency during the first half of March. Their temporal distribution coincided with the snowfall period and associated snowpack loading. Wet-snow avalanches (n = 24) occurred from late February to mid-April and likewise peaked during the first half of March. Their continuation into April coincided with rising air temperatures and snowpack depletion, conditions conducive to snowmelt and liquid-water infiltration.

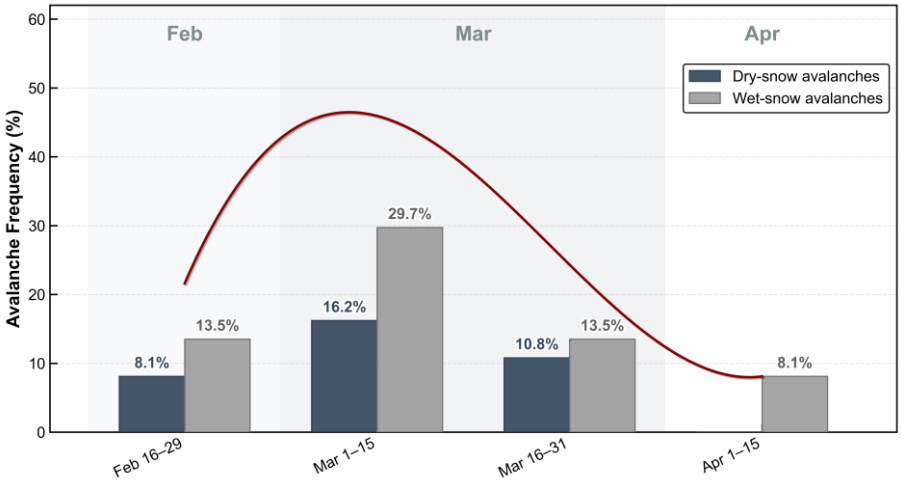


Figure 7. Seasonal distribution of avalanches. The bars show the frequencies of dry- and wet-snow avalanches in each half-month period, and the red curve represents a cubic-spline interpolation of their combined frequencies.

3.2 Model formulation and probabilistic relationships

3.2.1 Dry-snow avalanches

To establish a comparative baseline, we first constructed the dry-snow avalanche MOLM:

$$\ln\left(\frac{P}{1-P}\right) = -0.62 + 0.93\ln(1+\mathrm{SFI}) - 0.56\ln(1+\mathrm{SFD}), \quad (10)$$

In this baseline model, the regression coefficient for SFI is positive and statistically significant (95% CI [0.38, 1.52]), whereas the coefficient for SFD is negative but not statistically significant (95% CI [−1.36, 0.12]). A critical limitation of this model is that it defines a fixed decision boundary in the SFI–SFD phase space and is therefore independent of pre-event snow depth. Consequently, it assigns identical classification scores to conditions with the same SFI and SFD, regardless of differences in SD. To address this limitation, we incorporated SD as an additional predictor to construct the SMLM, formulated as follows:

$$\ln\left(\frac{P}{1-P}\right) = -0.78 + 0.55\ln(1+\mathrm{SFI}) - 0.62\ln(1+\mathrm{SFD}) + 1.93\ln(1+\mathrm{SD}), \quad (11)$$

In the dry-snow avalanche SMLM, the regression coefficient for SD is positive ($w_3 = 1.93$; 95% CI [1.07, 2.71]). Its confidence interval lies entirely above zero, indicating that greater pre-event snow depth is associated with a higher model-derived classification score when the other variables are held constant. The coefficient for SFI remains positive ($w_1 = 0.55$), but its bootstrap-derived 95% CI $[-0.03, 1.21]$ slightly overlaps zero. This indicates a positive but statistically uncertain effect after pre-event snow depth is incorporated into the model. Notably, the regression coefficient for SFD is negative and becomes statistically significant after SD is incorporated into the model ($w_2 = -0.62$; 95% CI $[-1.36, -0.02]$). This result indicates that, after accounting for pre-event snow depth, longer snowfall duration is associated with a lower model-derived classification score for dry-snow avalanches.

The modelling results (Fig. 8a) delineate the critical threshold surface for dry-snow avalanches within the three-dimensional parameter space of SFI, SFD, and SD. The optimal classification threshold, determined by maximising the Youden Index, is 0.41. This critical surface represents the modelled relationships between the three predictors and avalanche classification. An examination of the two-dimensional cross-sections reveals how the classification boundary varies with the individual predictors. Within the SFI–SD plane (Fig. 8b), a pronounced compensatory relationship between SFI and SD is evident. As SD increases, the critical SFI required to cross the model-derived threshold decreases substantially. Under conditions of a deep snowpack (high SD), even a marginal increment in SFI can drive the model prediction across the critical boundary into the above-threshold region. In the SFI–SFD plane (Fig. 8c), SFI has a strong influence on the classification outcome. When SFI is exceptionally high (> 10 mm/h), model-derived classification scores remain above the classification threshold across most of the plotted SFD range, rendering the influence of SFD variations largely negligible within the plotted range. However, at low-to-moderate SFI levels, the critical threshold line exhibits a positive slope with increasing SFD. This indicates that a higher SFI is required to reach the classification threshold as SFD increases. Finally, in the SFD–SD plane (Fig. 8d), at the fixed SFI shown, conditions with SD > 0.8 m fall within the above-threshold regime across the displayed SFD range. Conversely, the critical boundary shifts slightly upward as SFD increases. This indicates that SFD modifies the model-derived classification boundary in combination with SD and SFI.

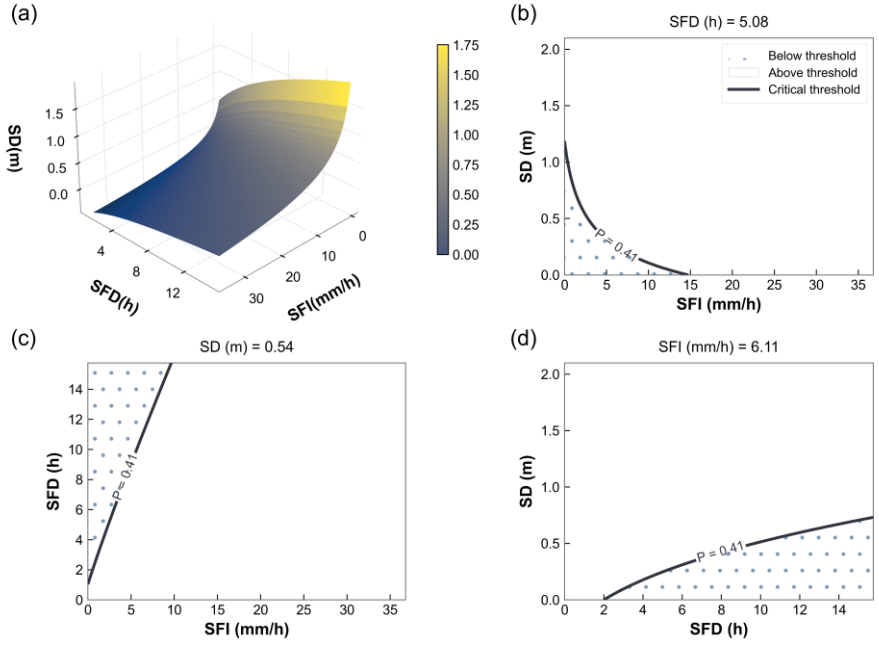


Figure 8. Three-dimensional (3D) visualization of the dry-snow avalanche SMLM classification boundary and its two-dimensional (2D) cross-sections. (a) The 3D surface represents the combinations of SFI, SFD, and SD at which the model-derived classification score equals the classification threshold (P = 0.41); the surface colour denotes SD. (b–d) 2D cross-sections of the model-derived threshold surface, with the third variable fixed at its mean value, as indicated above each panel. The black solid lines represent the classification boundary. The unpatterned white and blue-dotted regions indicate model-derived classification scores above and below the classification threshold, respectively.

3.2.2 Wet-snow avalanches

Analogous to the dry-snow avalanche analysis, we first constructed the wet-snow avalanche MOLM:

$$\ln\left(\frac{P}{1-P}\right) = -0.08 + 2.27\ \ln(1 + \mathrm{SMI}) - 0.93\ \ln(1 + \mathrm{SMD})\,, \tag{12}$$

In this baseline model, the regression coefficient for SMI is positive and statistically significant (95% CI [1.70, 2.82]), and the coefficient for SMD is negative and also statistically significant (95% CI [−1.63, −0.44]). However, as with the dry-snow MOLM, this baseline model does not account for the influence of varying pre-event snow depth on the model-derived critical boundary. To address this limitation, SD was incorporated as an additional predictor to construct the integrated wet-snow SMLM, formulated as follows:

$$\ln\left(\frac{P}{1-P}\right) = -0.25 + 1.37\ln(1 + \mathrm{SMI}) - 1.49\ln(1 + \mathrm{SMD}) + 2.68\ln(1 + \mathrm{SD})\,, \tag{13}$$

Within the wet-snow SMLM, the regression coefficient for SD is positive ($w_3 = 2.68\,; 95\%\ \mathrm{CI}\ [1.83, 3.40]$). Its confidence interval lies entirely above zero, indicating that greater pre-event snow depth is associated with a higher model-derived classification score when SMI and SMD are held constant. The coefficient for SMI is positive ($w_1 = 1.37; 95\%\ \mathrm{CI}\ [0.67, 2.02]$), indicating a positive association between melt intensity and wet-snow avalanche occurrence. Furthermore, the regression coefficient for SMD is negative ($w_2 = -1.49; 95\%\ \mathrm{CI}\ [-1.97, -1.10]$), indicating a negative association between snowmelt duration and wet-snow avalanche occurrence when SMI and SD are held constant.

The modelling results (Fig. 9a) delineate the model-derived critical surface for wet-snow avalanches within the three-dimensional feature space of SMI, SMD, and SD, with the optimal classification threshold identified as 0.49. The two-dimensional cross-sections further reveal that the three variables exert distinct influences on the position and shape of the critical boundary. Within the SMI–SD plane (Fig. 9b), the critical boundary exhibits a pronounced nonlinear decreasing trend. This pattern indicates that higher SMI increases the model-derived classification score, allowing it to exceed the classification threshold even when SD is relatively low. In the SMI–SMD plane (Fig. 9c), the critical boundary is characterised by a positive slope. High SMI can place conditions above the classification threshold even when SMD is relatively short. Conversely, under low-SMI conditions, the model-derived classification score tends to remain below the classification threshold even if SMD is prolonged. In the SMD–SD plane (Fig. 9d), when SMI is held constant, the critical boundary exhibits an overall nonlinear ascending trend with increasing SMD, indicating that a higher SD is required to reach the classification threshold as SMD increases. Overall, the wet-snow avalanche SMLM indicates that SMI, SMD, and SD jointly shape the model-derived critical threshold surface.

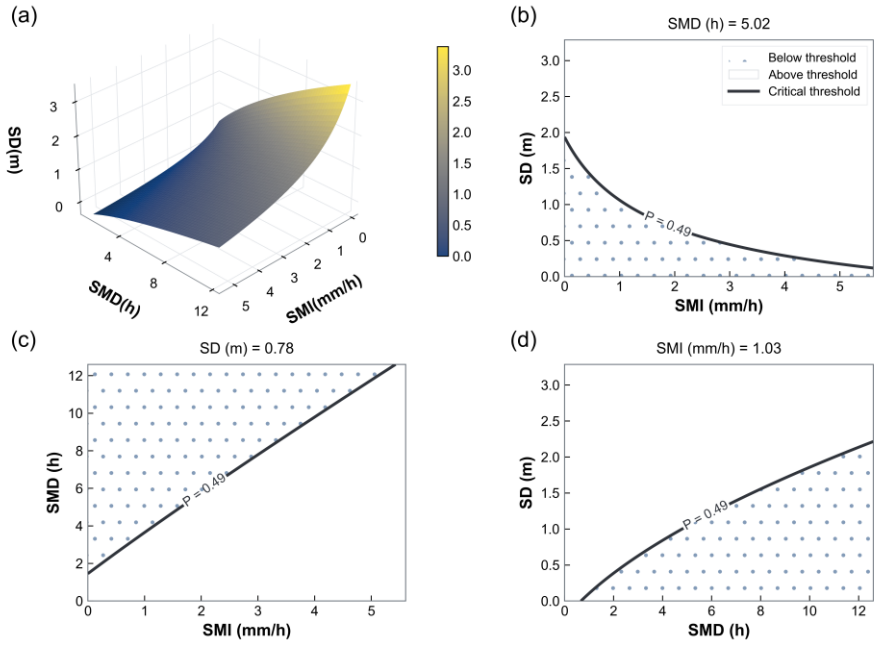


Figure 9. Three-dimensional (3D) visualization of the wet-snow avalanche SMLM classification boundary and its two-dimensional (2D) cross-sections. (a) The 3D surface represents the combinations of SMI, SMD, and SD at which the model-derived classification score equals the classification threshold (P = 0.49); the surface colour denotes SD. (b–d) 2D cross-sections of the model-derived threshold surface, with the third variable fixed at its mean value, as indicated above each panel. The black solid lines represent the classification boundary. The unpatterned white and blue-dotted regions indicate model-derived classification scores above and below the classification threshold, respectively.

3.3 Model performance

To assess the discriminative capacity of the SMLM, we compared its overall classification performance with that of the baseline MOLM using the LOOCV-derived predictions. The ROC curve analysis indicates that the SMLM consistently achieves better discrimination than the MOLM for both dry- and wet-snow avalanche scenarios (Fig. 10). Specifically, for dry-snow avalanches, the AUC increased from 0.72 (95% CI: 0.56–0.86) for the MOLM to 0.83 (95% CI: 0.71–0.94) for the SMLM. For wet-snow avalanches, the AUC increased from 0.85 (95% CI: 0.76–0.92) for the MOLM to 0.94 (95% CI: 0.88–0.99) for the SMLM. Paired bootstrap comparisons yielded AUC differences (SMLM − MOLM) of 0.11 (95% CI: 0.01–0.24) and 0.09 (95% CI: 0.02–0.17) for dry- and wet-snow avalanches, respectively.

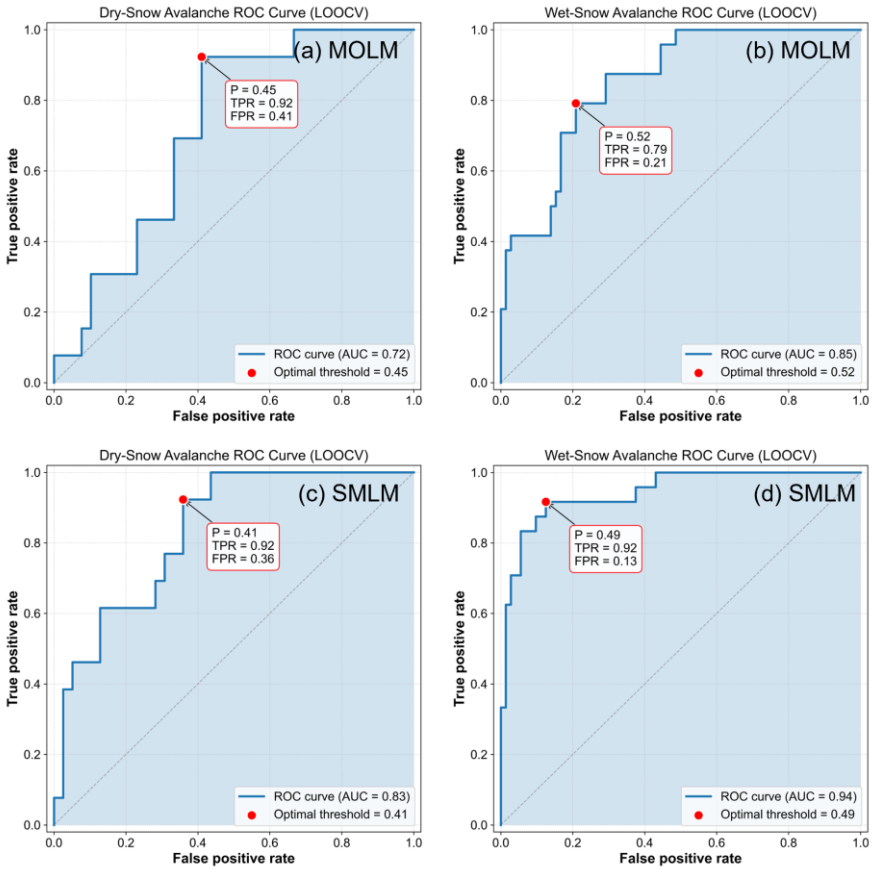


Figure 10. ROC curves and AUC comparison between the MOLM and SMLM for dry- and wet-snow avalanches under LOOCV. (a) Dry-snow avalanche MOLM; (b) wet-snow avalanche MOLM; (c) dry-snow avalanche SMLM; and (d) wet-snow avalanche SMLM. Red markers indicate the operating points at the optimal classification thresholds, with the corresponding TPR and FPR values shown.

The SMLM demonstrates a more effective trade-off between false alarms and missed events at the selected classification thresholds (Table 2). For wet-snow avalanches, the MOLM yields an FPR of 0.21 and a precision of 0.56. In contrast, the SMLM reduces the FPR to 0.13 while increasing precision to 0.71 and TPR from 0.79 to 0.92. For dry-snow avalanches, the FPR decreased from 0.41 to 0.36, while precision increased from 0.43 to 0.46. The TPR remained unchanged at 0.92. TSS increased from 0.58 to 0.79 for wet-snow avalanches and from 0.51 to 0.56 for dry-snow avalanches. The paired bootstrap TSS differences (SMLM − MOLM) were 0.21 (95% CI: 0.01–0.38) for wet-snow avalanches and 0.05 (95% CI: −0.08–0.19) for dry-snow avalanches.

Table 2. Comparison of classification performance metrics between the MOLM and SMLM.

	Wet MOLM	Dry MOLM	Wet SMLM	Dry SMLM
TPR (95% CI)	0.79 (0.64–0.95)	0.92 (0.75–1.00)	0.92 (0.77–1.00)	0.92 (0.75–1.00)
FPR (95% CI)	0.21 (0.12–0.31)	0.41 (0.25–0.57)	0.13 (0.06–0.21)	0.36 (0.20–0.51)
TSS (95% CI)	0.58 (0.39–0.77)	0.51 (0.27–0.71)	0.79 (0.64–0.91)	0.56 (0.33–0.77)
TNR	0.79	0.59	0.88	0.64
FNR	0.21	0.08	0.08	0.08
Precision	0.56	0.43	0.71	0.46
F1	0.66	0.59	0.80	0.62
TN/FP/FN/TP	57/15/5/19	23/16/1/12	63/9/2/22	25/14/1/12

4. Discussion

4.1 Physical interpretation of avalanche triggering

Avalanche activity is influenced by the combined effects of meteorological forcing and antecedent snow cover under different terrain conditions. The model results show that SD, representing pre-event snow depth, is positively associated with the model-derived relative likelihood of avalanche occurrence for both dry- and wet-snow avalanches. This finding is consistent with previous studies indicating that sufficient pre-existing snow cover can reduce the influence of terrain roughness on avalanche formation and affect the amount of new snow required for avalanche release (Schweizer et al., 2003a). Previous investigations of large avalanches affecting transportation corridors have also identified antecedent snow depth as a relevant factor in avalanche forecasting (Schweizer et al., 2009). These findings highlight the value of considering pre-event snow depth together with meteorological forcing when assessing recorded avalanche occurrence.

The models also show positive associations between forcing intensity and avalanche occurrence for both avalanche types, although the strength of statistical support differs. In the wet-snow avalanche model, the positive and statistically significant coefficient for SMI indicates that a greater rate of snow-depth loss during identified snowmelt-related processes is associated with a higher model-derived relative likelihood of wet-snow avalanche occurrence. This relationship is consistent with the role of liquid-water infiltration in wet-snow instability, where water movement through layered snow can alter snowpack mechanical properties and promote local water accumulation above melt–freeze crusts or capillary barriers (Conway and Raymond, 1993; Mitterer et al., 2011). By contrast, the positive coefficient for SFI in the dry-snow avalanche model is consistent with the role of snowfall loading, although its statistical support is weaker after SD is included. Snowfall increases the gravitational load on the existing snowpack, and rapid loading can promote instability when the rate of loading exceeds the rate of snowpack strengthening (Schweizer et al., 2003a). These relationships are consistent with the distinct physical processes associated with snowfall loading and melt-related changes in snowpack stability.

Previous studies have examined the time-dependent evolution of snowpack stability under meteorological loading, particularly the balance between loading rates and snow strength development (Conway and Wilbour, 1999; Schweizer et al., 2003a). Our modelling results indicate that both SFD for dry-snow avalanches and SMD for wet-snow avalanches are negatively associated with the model-derived relative likelihood of avalanche occurrence when forcing intensity and pre-event snow depth are held constant. For dry-snow avalanches, snowfall loading is accompanied by time-dependent processes, including settlement, compaction, sintering, and stress redistribution, which influence the evolution of snowpack stability during a snowfall episode (Schweizer et al., 2003a). For wet-snow avalanches, liquid-water infiltration and redistribution evolve over time, with snow stratigraphy, preferential flow paths, and local water accumulation influencing the development of wet-snow instability (Mitterer et al., 2011; Wever et al., 2016). These processes provide a physical context for the observed duration-related associations, highlighting the relevance of snowfall and snowmelt duration in distinguishing avalanche-event from non-event conditions.

4.2 Model discrimination

The comparison between the MOLM and SMLM reveals improvements in model discrimination for both dry- and wet-snow avalanches, although the changes in threshold-dependent performance differ. For wet-snow avalanches, incorporating SD improved the detection of avalanche-event samples and reduced false positives among non-event snowmelt processes, resulting in a substantial improvement in TSS. For dry-snow avalanches, the MOLM already identified most recorded avalanche events, and the inclusion of SD primarily reduced false positives, without changing the true-positive rate at the selected classification threshold. The improvements in AUC for both avalanche types further indicate that pre-event snow depth provides discriminatory information beyond meteorological forcing intensity and duration.

The benefit of combining meteorological forcing with snow-related information has also been demonstrated in previous avalanche modelling studies. For natural dry-snow avalanches, combining predictions based on snowfall amounts and simulated snowpack instability improved avalanche-day classification compared with either individual model (Mayer et al., 2023). In contrast to approaches that rely on detailed snowpack simulations, our results show that directly observed pre-event snow depth can provide additional discriminatory information when combined with forcing intensity and duration. By using a small set of readily available variables, the SMLM offers an observation-based approach to distinguishing avalanche-event and non-event conditions in data-limited mountain regions, providing a basis for the further development of locally adapted avalanche assessment methods.

4.3 Model-derived patterns and implications for avalanche early warning

The SMLM provides continuous classification scores based on pre-event snow depth and the intensity and duration of snowfall or snowmelt processes. These scores allow the model response to different combinations of predictors to be examined beyond a single binary classification threshold. For illustrative purposes, the model-derived scores were divided into five equal-width intervals (Fig. 11). The resulting three-dimensional patterns illustrate how model scores vary with meteorological forcing and

pre-event snow depth, and how different combinations of predictors can produce similar scores. Higher scores indicate predictor combinations more strongly associated with recorded avalanche events within the sampled data. These patterns provide an interpretable quantitative basis for identifying conditions associated with avalanche occurrence and informing the development of locally adapted avalanche early-warning criteria.

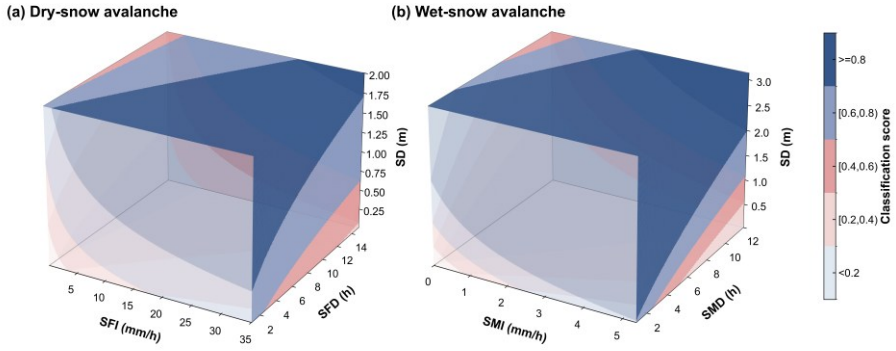


Figure 11. Illustrative three-dimensional classification-score intervals derived from the SMLM for (a) dry- and (b) wet-snow avalanches.

4.4 Limitations and future perspectives

The improved discrimination achieved by the SMLM highlights the value of combining pre-event snow depth with meteorological forcing, while the scope of the available observations places some limits on its broader application. The two-season record and the monitoring stations in Galongla Valley provide valuable local evidence, but do not encompass the full variability of snowpack and meteorological conditions across southeastern Tibet. Moreover, because model performance was assessed using LOOCV, its applicability to other locations and snow seasons remains to be established. At the methodological level, the LR framework estimates statistical associations between avalanche-event status and the predictors, rather than explicitly modelling the physical processes governing snowpack stability.

Future research should focus on extending the observational record and examining model performance across a wider range of locations and snow seasons. Incorporating snowpack stability indices or mechanistic constraints within the existing statistical structure could strengthen the physical interpretation of the identified relationships. Furthermore, spatially distributed meteorological and topographical information could help account for local environmental differences and support the adaptation of this observation-based approach to other mountain regions. Together, these developments would provide a basis for more widely applicable, locally adapted avalanche assessment methods.

5. Conclusions

In this study, we developed separate logistic regression models for dry- and wet-snow avalanches in Galongla Valley, southeastern Tibetan Plateau, combining pre-event snow depth with snowfall- or snowmelt-process variables. Using

observations from local monitoring stations during the 2024 and 2025 snow seasons, we examined avalanche-event and non-event conditions separately for the two avalanche types to account for their distinct meteorological forcing processes. The findings show that pre-event snow depth (SD) and forcing intensity (SFI/SMI) were positively associated with the model-derived relative likelihood of avalanche occurrence, whereas forcing duration (SFD/SMD) showed negative associations when intensity and SD were held constant.

Incorporating SD improved model discrimination for both avalanche types under LOOCV. Compared with the MOLM, the SMLM achieved a TPR of 0.92 for both dry- and wet-snow avalanches at the selected classification thresholds, increased the AUC from 0.72 to 0.83 for dry-snow avalanches and from 0.85 to 0.94 for wet-snow avalanches, and reduced the FPR from 0.41 to 0.36 and from 0.21 to 0.13, respectively. These results show that incorporating pre-event snow depth alongside snowfall- and snowmelt-process variables improves the identification of avalanche-event conditions for both avalanche types. Based on local observations from a region where avalanche studies remain limited, our findings provide a practical basis for refining avalanche monitoring and informing the development of locally adapted early-warning methods in Galongla Valley.

Code and data availability

The processed dataset used in this study, including meteorological indicators, snow depth, avalanche-type labels, and binary avalanche occurrence records, and the Python scripts used for the SMLM and MOLM modelling have been deposited in Zenodo at https://doi.org/10.5281/zenodo.23391913. The repository contains the input files and scripts required to reproduce the logistic regression modelling, leave-one-out cross-validation, model performance evaluation, and the key figures presented in this study. The raw high-resolution monitoring-station observations are not publicly available because of institutional confidentiality agreements and data-use restrictions. Nevertheless, the processed dataset provided in the repository preserves the key variables required for the analyses and is sufficient to reproduce the statistical modelling and evaluation results reported in this paper.

Author contributions

X.F. conducted the data processing, data analysis, figure preparation, and manuscript writing. J.H. supervised the research and contributed to manuscript review and editing. P.C. and Y.W. provided scientific guidance and contributed to manuscript revision. G.C. contributed to manuscript review. All authors read and approved the final manuscript.

Competing interests

The contact author has declared that none of the authors has any competing interests.

Acknowledgements

We thank the field teams involved in the avalanche observations and maintenance of the monitoring network.

Financial support

This work was supported by the Science and Technology Projects of the Xizang Autonomous Region, China (Grant No. XZ202601ZD0009), and the Strategic Priority Research Program of the Chinese Academy of Sciences (Grant No. XDB1390000).

References

Acharya, A., Steiner, J. F., Walizada, K. M., Ali, S., Zakir, Z. H., Caiserman, A., and Watanabe, T.: Review article: Snow and ice avalanches in High Mountain Asia – scientific, local and indigenous knowledge, Nat. Hazards Earth Syst. Sci., 23, 2569–2592, https://doi.org/10.5194/nhess-23-2569-2023, 2023.

Baggi, S. and Schweizer, J.: Characteristics of wet-snow avalanche activity: 20 years of observations from a high alpine valley (Dischma, Switzerland), Nat Hazards, 50, 97–108, https://doi.org/10.1007/s11069-008-9322-7, 2009.

Bellaire, S., Van Herwijnen, A., Mitterer, C., and Schweizer, J.: On forecasting wet-snow avalanche activity using simulated snow cover data, Cold Regions Science and Technology, 144, 28–38, https://doi.org/10.1016/j.coldregions.2017.09.013, 2017.

Conway, H. and Raymond, C. F.: Snow stability during rain, J. Glaciol., 39, 635–642, https://doi.org/10.3189/S0022143000016531, 1993.

Conway, H. and Wilbour, C.: Evolution of snow slope stability during storms, Cold Regions Science and Technology, 30, 67–77, https://doi.org/10.1016/S0165-232X(99)00009-9, 1999.

Efron, B. and Tibshirani, R.: Bootstrap methods for standard errors, confidence intervals, and other measures of statistical accuracy, Stat. Sci., 1, 54–75, https://doi.org/10.1214/ss/1177013815, 1986.

Fawcett, T.: An introduction to ROC analysis, Pattern Recognit. Lett., 27, 861–874, https://doi.org/10.1016/j.patrec.2005.10.010, 2006.

Fu, X., Hao, J., Cui, P., Wang, Y., and Chen, G.: Dataset and Python code supporting “Forecasting different types of avalanches based on snow depth and snowfall/snowmelt conditions on the Southeastern Tibetan Plateau” (Version 2.0), Zenodo [data set and code], https://doi.org/10.5281/zenodo.23391913, 2026.

Gauthier, F., Germain, D., and Hétu, B.: Logistic models as a forecasting tool for snow avalanches in a cold maritime climate: Northern Gaspésie, Québec, Canada, Nat Hazards, 89, 201–232, https://doi.org/10.1007/s11069-017-2959-3, 2017.

Hastie, T., Tibshirani, R., and Friedman, J.: The elements of statistical learning: Data mining, inference, and prediction, 2nd ed., Springer, New York, https://doi.org/10.1007/978-0-387-84858-7, 2009.

Hendrick, M., Techel, F., Volpi, M., Olevski, T., Pérez-Guillén, C., van Herwijnen, A., and Schweizer, J.: Automated prediction of wet-snow avalanche activity in the Swiss Alps, J. Glaciol., 69, 1365–1378, https://doi.org/10.1017/jog.2023.24, 2023.

LaChapelle, E. R.: The fundamental processes in conventional avalanche forecasting, J. Glaciol., 26, 75–84, https://doi.org/10.3189/S0022143000010601, 1980.

Li, C., Hao, J., Zhang, G., Wang, Y., Fang, H., Hou, W., and Cui, P.: Extreme snowfall variations in the southeastern Tibetan Plateau under warming climate, Atmos. Res., 311, 107690, https://doi.org/10.1016/j.atmosres.2024.107690, 2024.

Marienthal, A., Hendrikx, J., Birkeland, K. W., and Irvine, K. M.: Meteorological variables to aid forecasting deep slab avalanches on persistent weak layers, Cold Regions Science and Technology, 120, 227–236, https://doi.org/10.1016/j.coldregions.2015.08.007, 2015.

Mayer, S., Techel, F., Schweizer, J., and van Herwijnen, A.: Prediction of natural dry-snow avalanche activity using physics-based snowpack simulations, Nat. Hazards Earth Syst. Sci., 23, 3445–3465, https://doi.org/10.5194/nhess-23-3445-2023, 2023.

Mayer, S., Hendrick, M., Michel, A., Richter, B., Schweizer, J., Wernli, H., and van Herwijnen, A.: Impact of climate change on snow avalanche activity in the Swiss Alps, The Cryosphere, 18, 5495–5517, https://doi.org/10.5194/tc-18-5495-2024, 2024.

McClung, D. M.: Dry snow slab quasi-brittle fracture initiation and verification from field tests, J. Geophys. Res.: Earth Surf., 114, F01022, https://doi.org/10.1029/2007JF000913, 2009.

Mitterer, C. and Schweizer, J.: Analysis of the snow-atmosphere energy balance during wet-snow instabilities and implications for avalanche prediction, The Cryosphere, 7, 205–216, https://doi.org/10.5194/tc-7-205-2013, 2013.

Mitterer, C., Hirashima, H., and Schweizer, J.: Wet-snow instabilities: Comparison of measured and modelled liquid water content and snow stratigraphy, Ann. Glaciol., 52, 201–208, https://doi.org/10.3189/172756411797252077, 2011.

Morin, S., Horton, S., Techel, F., Bavay, M., Coléou, C., Fierz, C., Gobiet, A., Hagenmuller, P., Lafaysse, M., Mitterer, C., Monti, F., Müller, K., Pittman, M., Schirmer, M., Vionnet, V., and Schweizer, J.: Application of physical snowpack models in support of operational avalanche hazard forecasting: A status report on current implementations and prospects for the future, Cold Regions Science and Technology, 170, 102910, https://doi.org/10.1016/j.coldregions.2019.102910, 2020.

Pérez-Guillén, C., Techel, F., Hendrick, M., Volpi, M., van Herwijnen, A., Olevski, T., and Schweizer, J.: Data-driven automated predictions of the avalanche danger level for dry-snow conditions in Switzerland, Nat. Hazards Earth Syst. Sci., 22, 2031–2056, https://doi.org/10.5194/nhess-22-2031-2022, 2022.

Schweizer, J. and Föhn, P. M. B.: Avalanche forecasting — an expert system approach, J. Glaciol., 42, 318–332, https://doi.org/10.3189/S0022143000004172, 1996.

Schweizer, J., Jamieson, B. J., and Schneebeli, M.: Snow avalanche formation, Rev. Geophys., 41, 1016, https://doi.org/10.1029/2002RG000123, 2003a.

Schweizer, J., Kronholm, K., and Wiesinger, T.: Verification of regional snowpack stability and avalanche danger, Cold Regions Science and Technology, 37, 277–288, https://doi.org/10.1016/S0165-232X(03)00070-3, 2003b.

Schweizer, J., Kronholm, K., Jamieson, J. B., and Birkeland, K. W.: Review of spatial variability of snowpack properties and its importance for avalanche formation, Cold Regions Science and Technology, 51, 253–272, https://doi.org/10.1016/j.coldregions.2007.04.009, 2008.

Schweizer, J., Mitterer, C., and Stoffel, L.: On forecasting large and infrequent snow avalanches, Cold Regions Science and Technology, 59, 234–241, https://doi.org/10.1016/j.coldregions.2009.01.006, 2009.

Wei, H., Wang, Y., Wang, S., Hao, J., Chen, G., and Fu, X.: Study on the snowfall amount triggering regional avalanches in southeastern Tibet, Water, 17, 1631, https://doi.org/10.3390/w17111631, 2025.

Wen, H., Wu, X., Shu, X., Wang, D., Zhao, S., Zhou, G., and Li, X.: Spatial heterogeneity and temporal tendency of channeled snow avalanche activity retrieved from Landsat images in the maritime snow climate of the Parlung Tsangpo catchment, southeastern Tibet, Cold Regions Science and Technology, 223, 104206, https://doi.org/10.1016/j.coldregions.2024.104206, 2024.

Wever, N., Würzer, S., Fierz, C., and Lehning, M.: Simulating ice layer formation under the presence of preferential flow in layered snowpacks, The Cryosphere, 10, 2731–2744, https://doi.org/10.5194/tc-10-2731-2016, 2016.

Youden, W. J.: Index for rating diagnostic tests, Cancer, 3, 32–35, https://doi.org/10.1002/1097-0142(1950)3:1%3C32::AID-CNCR2820030106%3E3.0.CO;2-3, 1950.

Yuan, X., Yang, K., Lu, H., Wang, Y., and Ma, X.: Impacts of moisture transport through and over the Yarlung Tsangpo Grand Canyon on precipitation in the eastern Tibetan Plateau, Atmospheric Research, 282, 106533, https://doi.org/10.1016/j.atmosres.2022.106533, 2023.

Zuur, A. F., Ieno, E. N., and Elphick, C. S.: A protocol for data exploration to avoid common statistical problems, Methods Ecol. Evol., 1, 3–14, https://doi.org/10.1111/j.2041-210X.2009.00001.x, 2010.